

Article

Simultaneous Catalytic Oxidation of Benzene and Toluene over Pd-CeZrO_x Catalysts

Xin Xing¹, Yixin Wang¹, Meiping Hao², Zhe Li¹, Dandan Liu¹ and Kezhou Yan^{2,*}

¹ College of Environment and Resources, Taiyuan University of Science and Technology, Taiyuan 030024, China; xingxin_1993@163.com (X.X.); s202323211124@stu.tyust.edu.cn (Y.W.); s202223211086@stu.tyust.edu.cn (Z.L.); liudd@tyust.edu.cn (D.L.)

² Institute of Resources and Environmental Engineering, Shanxi University, Taiyuan 030031, China; 202424003008@email.sxu.edu.cn

* Correspondence: yankz@sxu.edu.cn

Abstract: Since actual industrial emissions contain a wide range of volatile organic compounds, studies into the simultaneous catalytic degradation of multi-component VOCs are essential. This work developed Pd-CeZrO_x samples for the simultaneous elimination of benzene and toluene. Firstly, CeZrO_x supports were synthesized using several methods (co-precipitation, CTAB template co-precipitation, and sol-gel method). Pd active species were then added into the 1.0Pd-CeZrO_x samples using the impregnation procedure. XRD, BET, NH₃-TPD, Raman, EPR, XPS, and H₂-TPR were utilized to analyze the as-prepared Pd-CeZrO_x samples. The catalytic performance tests reveal that the performance of 1.0Pd-CeZrO_x-CTAB outperforms that of 1.0Pd-CeZrO_x-PM and 1.0Pd-CeZrO_x-CASG, and 1.0Pd-CeZrO_x-CTAB displays superior catalytic activity for both benzene and toluene oxidation. The improved redox properties, the abundant surface oxygen vacancies, and the surface Pd²⁺ species of the 1.0Pd-CeZrO_x-CTAB sample may be responsible for the simultaneous degradation activity of benzene and toluene.

Keywords: VOCs; benzene and toluene; simultaneous catalytic oxidation; Pd-CeZrO_x



Citation: Xing, X.; Wang, Y.; Hao, M.; Li, Z.; Liu, D.; Yan, K. Simultaneous Catalytic Oxidation of Benzene and Toluene over Pd-CeZrO_x Catalysts. *Atmosphere* **2024**, *15*, 1301. <https://doi.org/10.3390/atmos15111301>

Academic Editor: Kumar Vikrant

Received: 15 October 2024

Revised: 25 October 2024

Accepted: 28 October 2024

Published: 29 October 2024



Copyright: © 2024 by the authors. Licensee MDPI, Basel, Switzerland. This article is an open access article distributed under the terms and conditions of the Creative Commons Attribution (CC BY) license (<https://creativecommons.org/licenses/by/4.0/>).

1. Introduction

One of the primary contaminants in the atmosphere is volatile organic compounds (VOCs), which make significant contributions to the generation of secondary organic aerosols and ozone. Aromatic hydrocarbons, including benzene, toluene, xylene, and polycyclic aromatic hydrocarbons, are typical VOCs that exist in the petrochemical industry and coking coal production process [1]. Most aromatic hydrocarbons are harmful to both human health and the environment, and long-term exposure may lead to cancer. In addition, the composition of exhaust gases from industrial emission processes is complex and generally not a single component [2]. Therefore, benzene and toluene, as pollutants with high emissions, have received widespread attention from researchers.

The treatment technology of VOCs mainly includes two categories: recovery and destruction. The former includes the absorption method, adsorption method, and condensation method, while the latter includes direct combustion, catalytic oxidation, photocatalysis, plasma treatment, etc. [3]. Catalytic oxidation has been recognized as the most promising strategies to reduce VOCs because of its great effectiveness, energy efficiency, and the absence of secondary pollutants [4]. Catalysts are critical components of catalytic oxidation technology, which frequently includes both noble and non-noble metal samples. Catalysts with noble metal (Pt, Pd, Ru, etc.) have been selected over various non-noble metal oxides, considering the superior efficacy and selectivity [5].

The selection of the carrier plays an important role for noble metal catalysts. The carrier affects the valence state of the active center, which influences catalytic performance, particularly at low temperatures. Metal oxides, including Al₂O₃, ZrO₂, TiO₂, CeO₂, and

zeolite porous materials, as well as inorganic nonmetallic compounds such as SiO₂ and active carbon materials, are widely employed as carrier materials for dispersing noble metal [6–8].

CeO₂ possesses excellent oxygen storage and release capability, and the catalysts based on CeO₂ have rich oxygen vacancies, demonstrating significant activity and selectivity for the oxidation of VOCs. Ce_xMn_{1-x}O₂ catalysts exhibited higher catalytic activities for toluene oxidation, corresponding to the ability of oxygen vacancies to drive the rate-determining phase of toluene oxidation [9]. For the oxidation of toluene, a range of CeO₂-based catalysts loaded with Pt_xIr was prepared, and the exceptional catalytic properties may be due to the synergy between Pt and Ir species, a higher concentration of surface oxygen vacancies, and improved reducibility at low temperatures [10]. Wang et al. prepared Pt-Pd/CeO₂ samples, which exhibit superb catalytic performance for the degradation of toluene, and surface Ce³⁺ and oxygen vacancies were activation sites [11]. Moreover, it has been demonstrated that the addition of ZrO₂ into CeO₂ enhances its redox abilities and oxygen storage capacity [12,13]. Additionally, CeZrO₂ could enhance the distribution of the metal species on the supports, which has a beneficial influence on enhancing catalytic activity [14]. Ag/CeZrO₂ catalysts were prepared to study the catalytic activity of toluene oxidation, and the sample with a Ce/Zr ratio of 1:1 displayed the greatest catalytic activity (T₉₀ = 240 °C) [15]. Zheng et al. prepared sulfated CeZrO_x-loaded platinum samples and tested for toluene oxidation; the tolerance to SO₂ poisoning was greatly improved, which might be linked to the greater surface acidity [16].

Based on the foregoing, it is proposed to perform an extensive study on the simultaneous catalytic degradation of benzene and toluene utilizing highly active Pd catalysts. A series of Pd-CeZrO_x samples with high synergistic catalytic activity were synthesized by the impregnation method. The catalytic conversion of multi components (benzene and toluene) and CO₂ selectivity were evaluated over these samples at 100–350 °C. The physical properties were investigated by X-ray diffraction (XRD) and N₂ adsorption–desorption. X-ray photoelectron spectroscopy (XPS) was employed for studying the elements' valence state changes; Raman and electron paramagnetic resonance (EPR) were used for the characterization of oxygen vacancies. The redox ability and acid sites were investigated by H₂ temperature-programmed reduction (H₂-TPR) and NH₃ temperature-programmed desorption (NH₃-TPD). By elucidating the structure-activity relationship for the simultaneous catalytic degradation of benzene and toluene, this study could offer novel perspectives into the design of VOCs simultaneous catalytic degradation materials.

2. Materials and Methods

2.1. Chemicals and Raw Materials

The cerium nitrate hexahydrate (Ce(NO₃)₃·6H₂O, 99.99%) and zirconium nitrate pentahydrate (Zr(NO₃)₄·5H₂O, AR) were purchased from Macklin Technology (Shanghai, China). Citric acid monohydrate (C₆H₈O₇·H₂O, 99.5%) was bought from Sinopharm Chemical Reagent (Shanghai, China); cetyl trimethyl ammonium bromide (CTAB, C₁₉H₄₂BrN, 99.0%), ammonia (NH₃·H₂O, 25–28%), and anhydrous ethanol (CH₃CH₂OH, 99.7%) were obtained from Tianjin Tianli Chemical Reagent (Tianjin, China). Without additional purification, every chemical was used just as it was received. Deionized water was made inside the laboratory.

2.2. Synthesis of Catalysts

2.2.1. Synthesis of CeZrO_x

Synthesis of CeZrO_x by the ordinary co-precipitation method: 4.34 g Ce(NO₃)₃·6H₂O and 4.29 g Zr(NO₃)₄·5H₂O were dissolved in 100 mL deionized water and mixed well; ammonia solution with a mass concentration of 25% was added dropwise to control the pH of the solution to 10, and it was stirred for 2 h. The solution was filtered and washed with deionized water to pH 7, dried at 120 °C for 12 h, and then calcined (600 °C, 10 °C/min heating rate) for 4 h to obtain CeZrO_x-PM.

Synthesis of CeZrO_x by the CTAB template co-precipitation method: 4.34 g Ce(NO₃)₃·6H₂O and 4.29 g Zr(NO₃)₄·5H₂O were dissolved in 100 mL deionized water and mixed well, and the mixture was added dropwise to 60 mL C₁₉H₄₂BrN solution with a mass concentration of 151.8 mg/mL. The pH was controlled to 11 with ammonia, and the mixture was stirred for 2 h, filtered, and washed with 500 mL deionized water and 500 mL anhydrous ethanol, dried at 120 °C for 12 h, and then calcined (600 °C, 10 °C/min heating rate) for 4 h to obtain CeZrO_x-CTAB.

Synthesis of CeZrO_x by citric acid sol-gel method: 4.34 g Ce(NO₃)₃·6H₂O and 4.29 g Zr(NO₃)₄·5H₂O in a molar ratio of 1:1 were dissolved in 100 mL deionized water and mixed into an equimolar amount of 60 mL C₆H₈O₇·H₂O solution with a mass concentration of 140.2 mg/mL; the obtained mixture was stirred and evaporated to a transparent gel at 95–100 °C; the gel solid was dried at 120 °C for 12 h and then calcined (600 °C, 10 °C/min heating rate) for 4 h. Lastly, the CeZrO_x-CASG was obtained.

2.2.2. Impregnation of CeZrO_x

CeZrO_x-PM was impregnated with 0.1%, 0.5%, 1.0%, and 2.0% Pd solutions. Then, 4 g CeZrO_x-PM was weighted separately and placed in four beakers; 0.679, 3.397, 6.795, and 13.59 mL of Pd solution (5.886 mg/mL) were added to the four beakers and stirred well. After ultrasonic treating at room temperature for 15 min, the obtained impregnated samples were dried at 100 °C for 12 h. Eventually, they were calcined (600 °C, 10 °C/min heating rate) for 4 h to obtain samples with different impregnation amounts, denoted as 0.1Pd-CeZrO_x-PM, 0.5Pd-CeZrO_x-PM, 1.0Pd-CeZrO_x-PM, and 2.0Pd-CeZrO_x-PM.

Then, 4 g of CeZrO_x-CTAB and 4 g of CeZrO_x-CASG were placed in two beakers, and 6.795 mL of Pd solution was added to the two beakers, respectively. The specific impregnation method is the same as above. The impregnated samples obtained were 1.0Pd-CeZrO_x-CTAB and 1.0Pd-CeZrO_x-CASG.

2.3. Materials Characterization

The crystal structures of the catalysts were analyzed using an XRD with a Cu K α source (D8 Advance, Bruker, Germany). Scanning 2 θ degrees ranged from 10° to 80° at a rate of 5°/min.

A Micromeritics ASAP 2020 gas adsorption analyzer was used to characterize N₂ adsorption-desorption of the sample. The catalysts underwent a 6 h degassing process at 300 °C prior to the N₂ adsorption measurement.

The Raman spectra were tested by a LabRam HR Evolution Raman spectrometer with a 532 nm excitation wavelength. The frequency range tested was 100–1000 cm⁻¹.

Using an X-band Bruker EMX spectrometer, EPR spectra were measured at 77 K; 20 mg samples were inserted in a quartz probe cell equipped with greaseless stopcocks.

A chemisorption analyzer (Chemisorb 2920, Micromeritics, Norcross, GA, USA) with a thermal conductivity detector (TCD) was used to perform the H₂-TPR. Following a 1 h pretreatment at 300 °C with a flow rate of 20 mL/min He, 50 mg of samples were reduced at a flow rate of 50 mL/min with 2% H₂/He. The temperature was set at 800 °C with a heating rate of 10 °C/min.

NH₃-TPD experiments were also completed by a Micromeritics Chemisorb 2920 chemisorption analyzer. The NH₃-TPD testing process was as follows: 0.1 g of sample was pretreated in He flow at 300 °C for 1 h with a heating rate of 10 °C/min before being cooled down to room temperature. Subsequently, He was switched to NH₃ for adsorption for 30 min at a flow rate of 50 mL/min. Then, He was purged to eliminate the remaining NH₃ in the sample tube and prevent physical adsorption on the catalyst. The catalyst was heated to 700 °C at a rate of 10 °C/min in a He atmosphere for desorption, and mass spectrometry (MS) was used to identify the desorbed NH₃ signal.

XPS was measured using a XPS spectrometer (ESCALAB 250XI, Thermo Fisher Scientific, Waltham, MA, USA). The electron binding energy of the measured elements was corrected by C 1 s binding energy (284.6 eV).

2.4. Catalytic Activity Evaluation

A fixed bed quartz reactor running at atmospheric pressure was used to evaluate the catalyst activity. The experiments utilized 0.5 mL of catalyst with a particle size ranging from 40 to 60 mesh. The overall flow rate was 150 mL/min, and the gas hourly space velocity (GHSV) was 18,000 h⁻¹. The reaction gas contained 250 ppm of benzene, 250 ppm of toluene, and 5 vol% of O₂ and N₂ for balance. The catalytic activity was tested at a temperature ranging from 100 °C to 400 °C. The concentrations of feed and reaction gases were measured with a portable gas chromatograph (GC 7960 plus, Allen analyzer, Tengzhou, China). The gas chromatograph's column box temperature was 100 °C, and the CB-TVOC capillary column was used to separate benzene and toluene, and the detection of CO and CO₂ was carried out by an FID detector equipped with a reformer furnace. The pertinent experimental data were computed using Equations (1)–(3):

$$\text{Benzene conversion (\%)} = \frac{\text{benzene (in)} - \text{benzene (out)}}{\text{benzene (in)}} \times 100 \quad (1)$$

$$\text{Toluene conversion (\%)} = \frac{\text{toluene (in)} - \text{toluene (out)}}{\text{toluene (in)}} \times 100 \quad (2)$$

$$\text{CO}_2 \text{ selectivity (\%)} = \frac{\text{CO}_2 \text{ (ppm)}}{\text{Total product C (ppm)}} \times 100 \quad (3)$$

3. Results and Discussion

3.1. Structural Characterization

The XRD patterns of 1.0Pd-CeZrO_x-PM, 1.0Pd-CeZrO_x-CTAB, and 1.0Pd-CeZrO_x-CASG are shown in Figure 1. For all of the samples, the specific signals encountered at 29.25°, 34.03°, 48.90°, and 58.02° correlated with the (101), (110), (200), and (211) planes of Ce_{0.5}Zr_{0.5}O₂ (JCPDS 38-1436) [17]. The XRD pattern shows the decrease in Ce_{0.5}Zr_{0.5}O₂ lattice parameters caused by Zr⁴⁺ tiny ions (0.84 Å) replacing Ce⁴⁺ species (0.97 Å). This indicates that Zr cations have been completely incorporated into the CeO₂ lattice to produce a homogenous solid solution [18]. There are no reflections found that correspond to the phases of Pd or PdO species, which suggests the presence of tiny particles (<4 nm) [19]. In contrast, the diffraction peak intensity of the 1.0Pd-CeZrO_x-CASG sample is stronger, indicating that the CeZrO_x prepared by the citric sol-gel method has a larger grain size and stronger crystallinity. The weaker diffraction peaks of the traditional co-precipitation method and the CTAB template co-precipitation method suggest that the CeZrO_x formed using these two methods has a smaller grain size and lower crystallinity [20].

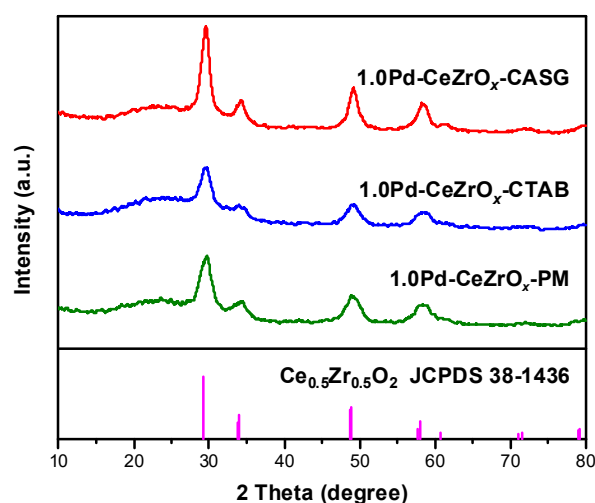


Figure 1. XRD patterns for 1.0Pd-CeZrO_x catalysts.

The specific surface area (SSA) and pore structure parameters of series 1.0Pd-CeZrO_x samples were analyzed by N₂ adsorption–desorption (Table 1). The SSA decreased with a drop in this order: 1.0Pd-CeZrO_x-PM (78.24 m²/g) > 1.0Pd-CeZrO_x-CTAB (72.08 m²/g) > 1.0Pd-CeZrO_x-CASG (13.08 m²/g), and there is also a similar trend of the pore volume: 1.0Pd-CeZrO_x-PM (0.07 cm³/g) > 1.0Pd-CeZrO_x-CTAB (0.06 m³/g) > 1.0Pd-CeZrO_x-CASG (0.04 m³/g). Compared with 1.0Pd-CeZrO_x-PM and 1.0Pd-CeZrO_x-CTAB, 1.0Pd-CeZrO_x-CASG possesses the highest pore size, whereas other samples have pore sizes about 3 nm, belonging to the mesoporous structure. Figure 2 clearly shows that all the samples demonstrated a type IV isotherm with the distinctive hysteresis loops, confirming the existence of a mesoporous structure [21]. Differently, 1.0Pd-CeZrO_x-CTAB and 1.0Pd-CeZrO_x-CASG samples show type H2 hysteresis loops with ink-bottle pores [22], while the 1.0Pd-CeZrO_x-PM sample exhibits an H3 hysteresis loop, which corresponds to a system with capillary coalescence in the porous sorbent [23,24]. The foregoing characterization implies the series of CeZrO_x substrates contains certain structural differences.

Table 1. Textual properties data of 1.0Pd-CeZrO_x catalysts.

Sample	SSA (m ² /g)	Pore Volume (cm ³ /g)	Pore Size (nm)
1.0Pd-CeZrO _x -CASG	13.08	0.04	10.53
1.0Pd-CeZrO _x -CTAB	72.08	0.06	3.41
1.0Pd-CeZrO _x -PM	78.24	0.07	3.39

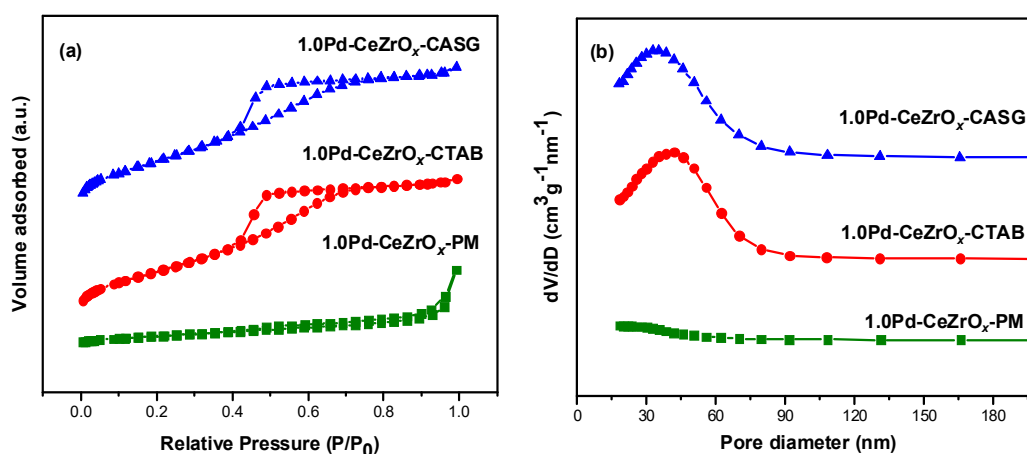


Figure 2. (a) N₂ adsorption-desorption curves of 1.0Pd-CeZrO_x catalysts; (b) the pore size distribution curve of 1.0Pd-CeZrO_x catalysts.

3.2. Evaluation of Catalytic Activity

3.2.1. Effect of Different Impregnation Amounts on Catalytic Activity

Firstly, the influence of Pd loading on catalytic activity was investigated. CeZrO_x as the carrier was synthesized by the precipitation method, and varied amounts of Pd were impregnated to produce a series of Pd-CeZrO_x-PM samples, and the simultaneous catalytic degradation performance of benzene and toluene were carried out over Pd-CeZrO_x-PM samples. Figure 3a shows the temperature-dependent benzene conversion during the benzene and toluene catalytic elimination using Pd-CeZrO_x-PM samples with different Pd impregnation amounts. It can be seen that all samples exhibit a uniform trend, and the benzene conversion rate increases continuously with increasing temperature. In addition, the benzene conversion shows significant changes with various loading amounts of Pd. At a temperature of 350 °C, 0.5Pd-CeZrO_x-PM, 1.0Pd-CeZrO_x-PM, and 2.0Pd-CeZrO_x-PM catalysts could achieve complete oxidation of benzene, while for the 0.1Pd-CeZrO_x sample, complete oxidation of benzene was achieved at 500 °C. Among these catalysts, the 0.1Pd-CeZrO_x-PM showed the worst catalytic activity, which indicated that the loading amount

of Pd is crucial for the catalytic oxidation activity of the samples, and the higher the loading amount, the better the catalytic conversion of the catalyst.

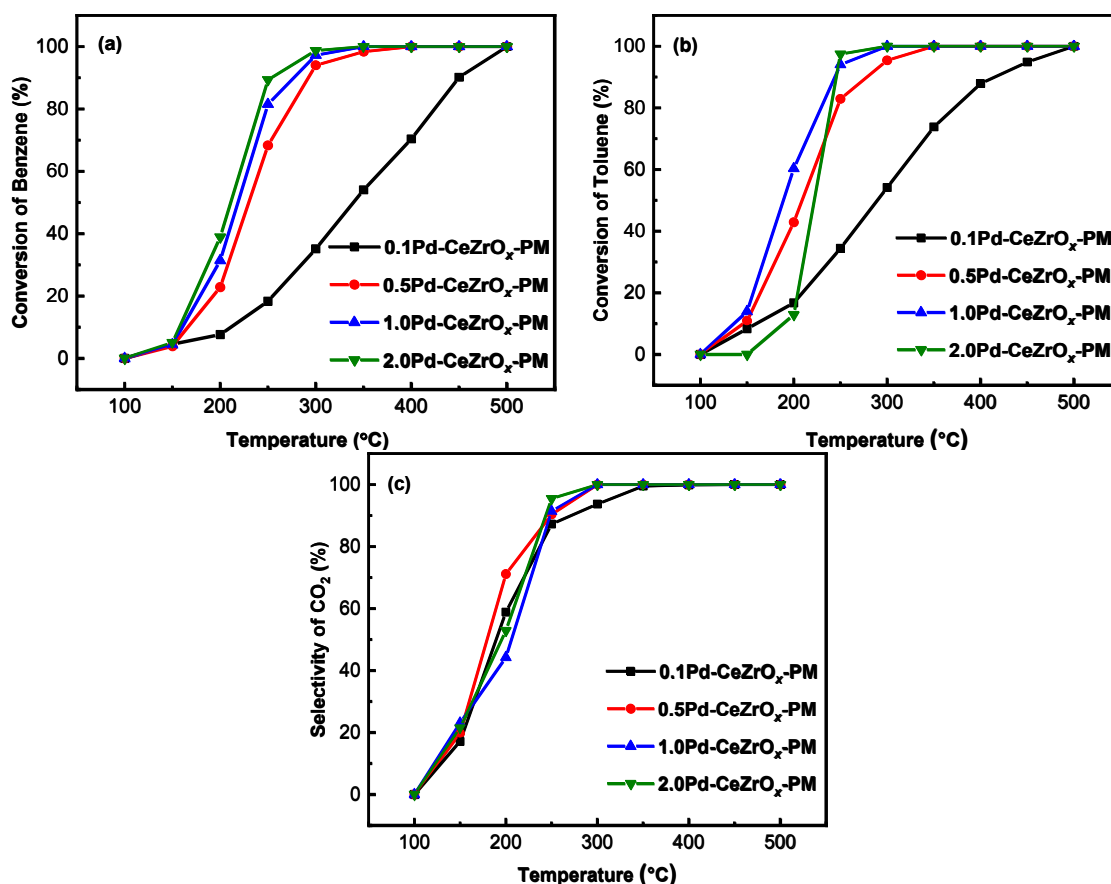


Figure 3. The synergistic catalytic oxidation performance of benzene and toluene over Pd-CeZrO_x-PM samples with different Pd content: (a) benzene conversion; (b) toluene conversion; (c) CO₂ selectivity.

Figure 3b shows the toluene conversion of Pd-CeZrO_x-PM samples in the multi-component VOCs (benzene and toluene). The toluene conversion rate over Pd-CeZrO_x-PM samples with Pd loading of 0.1%, 0.5%, and 1.0% increased with the temperature increasing until achieving the complete conversion of toluene. The primary temperature of toluene oxidation over the 2.0Pd-CeZrO_x-PM sample was 200 °C, which is higher than that of other samples. The complete conversion of toluene over 2.0Pd-CeZrO_x-PM was achieved at 250 °C; it was lower than other samples, suggesting the superior catalytic performance of 2.0Pd-CeZrO_x-PM samples. The temperature for achieving 100% toluene conversion from low to high over a series of Pd-CeZrO_x-PM materials is as follows: 2.0Pd-CeZrO_x-PM (250 °C) < 1.0Pd-CeZrO_x-PM (300 °C) < 0.5Pd-CeZrO_x-PM (350 °C) < 0.1Pd-CeZrO_x-PM (500 °C). It is worth noting that before 250 °C, 1.0Pd-CeZrO_x-PM exhibited superior catalytic performance. For the catalytic oxidation of toluene, 2.0Pd-CeZrO_x-PM with high Pd loading failed to exhibit strong low-temperature activity.

There are several intermediate compounds produced during the simultaneous catalytic elimination of benzene and toluene. Considering no CO was observed during the process, Figure 3c depicts the variation curve of CO₂ selectivity in the simultaneous catalytic elimination of benzene and toluene. As the temperature increases, the selectivity of CO₂ also shows an increasing trend. When the reaction temperature is raised to 300 °C, 0.5Pd-CeZrO_x-PM, 1.0Pd-CeZrO_x-PM, and 2.0Pd-CeZrO_x-PM samples all achieve 100% selectivity for CO₂. However, for the 1.0Pd-CeZrO_x-PM sample, a temperature of 350 °C is required to achieve 100% CO₂ selectivity.

In summary, the loading amount of Pd has a significant impact on the simultaneous catalytic elimination of benzene and toluene. For the catalytic degradation of benzene, the benzene conversion rate continuously increases with an increase in the loading amount; 1.0Pd-CeZrO_x-PM and 2.0Pd-CeZrO_x-PM catalysts could achieve complete oxidation of benzene at 350 °C. For the catalytic oxidation of toluene, the 1.0Pd-CeZrO_x-PM sample exhibits better catalytic performance at low temperatures; 1.0Pd-CeZrO_x-PM and 2.0Pd-CeZrO_x-PM catalysts could achieve complete oxidation of toluene at 300 °C. Additionally, considering the high cost of precious metal catalysts, while meeting the conversion rate of benzene catalytic degradation, a relatively moderate loading amount should be selected to achieve the target conversion rate while keeping the catalyst cost as low as feasible. As a result, a 1.0% impregnation of precious metal was chosen, and the effect of various carrier synthesis methods on the catalytic degradation performance of the materials were investigated.

3.2.2. Effect of Different Preparation Methods on Catalytic Activity

The carrier is critical for dispersing the catalyst's active phase. As a result, a number of CeZrO_x carrier materials were synthesized employing various preparation methods. Benzene and toluene were employed to test the catalytic performance of 1.0Pd-CeZrO_x samples, and the characteristic temperatures for the simultaneous catalytic elimination of benzene and toluene are shown in Table 2. The benzene and toluene conversion of the series samples rapidly increases with temperature in the range of 150–250 °C. The order of T₈₀ and T₁₀₀ from low to high is 1.0Pd-CeZrO_x-CTAB > 1.0Pd-CeZrO_x-PM > 1.0Pd-CeZrO_x-CASG. The characteristic temperature (T₈₀) corresponding to a toluene oxidation is lower than that corresponding to benzene oxidation, indicating that toluene molecules are relatively active and easily break bonds and rings during the catalytic oxidation process, further catalyzing degradation to produce CO₂ and H₂O.

Table 2. Catalytic activity of 1.0Pd-CeZrO_x catalysts.

Sample	Catalytic Benzene Activity (°C)		Catalytic Toluene Activity (°C)	
	T ₈₀	T ₁₀₀	T ₈₀	T ₁₀₀
1.0Pd-CeZrO _x -CASG	207	250	137	250
1.0Pd-CeZrO _x -CTAB	249	350	242	300
1.0Pd-CeZrO _x -PM	237	300	230	300

Figure 4a shows that the benzene conversion of 1.0Pd-CeZrO_x-CTAB was 80% at around 200 °C and complete at 250 °C. The complete conversion temperature of the 1.0Pd-CeZrO_x-PM catalyst was at 300 °C, while the complete conversion temperature of 1.0Pd-CeZrO_x-CASG was at 350 °C. As a result, the 1.0Pd-CeZrO_x sample synthesized by the CTAB template approach outperforms the other two ways in terms of benzene catalytic degradation. Figure 4b shows the curve of the conversion rate of toluene catalyzed by 1.0Pd-CeZrO_x samples over time, and the toluene conversion increases with increasing temperature. As shown in the figure, the toluene conversion rate reached 80% at around 140 °C for 1.0Pd-CeZrO_x-CTAB, and toluene was completely converted at 250 °C; the 1.0Pd-CeZrO_x-PM and 1.0Pd-CeZrO_x-CASG samples achieved complete conversion of toluene at 300 °C; similar to the catalytic oxidation process of benzene, the CeZrO_x support prepared by the co-precipitation method using the CTAB template showed superior performance in degrading toluene compared to those of other samples. Figure 4c depicts the temperature-dependent selectivity of CO₂ during the catalytic elimination of benzene and toluene using a series of 1.0Pd-CeZrO_x materials. With an increase in temperature, the CO₂ selectivity gradually increases, reaching 100% CO₂ selectivity at 250–300 °C. The CO₂ selectivity curves of the 1.0Pd-CeZrO_x-CTAB, 1.0Pd-CeZrO_x-PM, and 1.0Pd-CeZrO_x-CASG samples show similar trends. Among them, the CO₂ selectivity of the 1.0Pd-CeZrO_x-CASG sample is poor, which can be attributed to the generation of other organic by-products. It is worth

noting that there is no generation of CO throughout the entire reaction process. In addition, when the full conversion temperature is reached, carbon balance can be basically achieved ($98 \pm 2\%$).

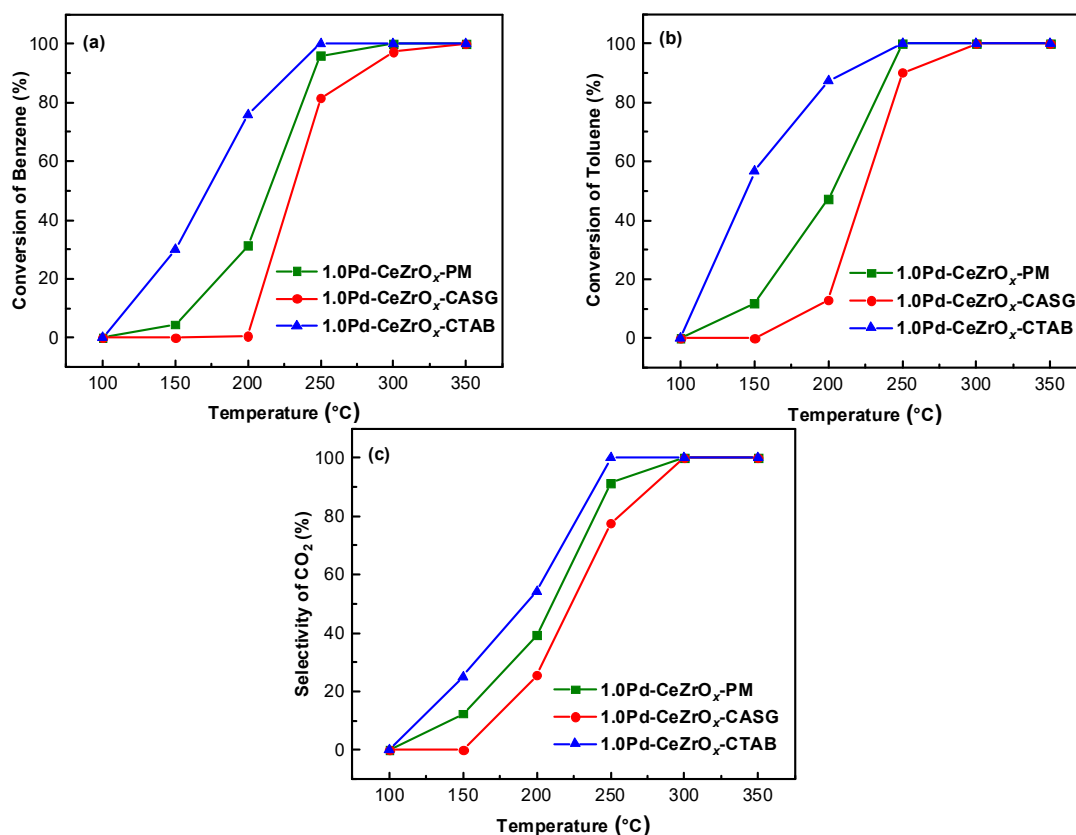


Figure 4. The simultaneous catalytic oxidation performance of benzene and toluene over 1.0Pd-CeZrO_x samples; (a) benzene conversion; (b) toluene conversion; (c) CO₂ selectivity.

In brief, the 1.0Pd-CeZrO_x-CTAB sample has the greatest catalytic performance, outperforming the 1.0Pd-CeZrO_x-CASG and 1.0Pd-CeZrO_x-PM samples. The 1.0Pd-CeZrO_x-CTAB catalyst could achieve benzene and toluene simultaneous catalytic degradation at 250 °C, while CO₂ selectivity reaches 100%. The catalytic performance of the 1.0Pd-CeZrO_x catalyst prepared by the CTAB template is better than that of the common co-precipitation method and the citric acid sol-gel method.

3.3. Acidity of Catalysts

The adsorption of pollutants is influenced by the acidity of the catalysts' surface. Consequently, NH₃-TPD was utilized to describe the acid sites of as-prepared samples (see Figure 5). Three samples showed two types of desorption peaks at 50–700 °C, attributed to weak and moderate acid sites with desorption temperatures ranging from 90 °C to 200 °C and 200 °C to 300 °C [16]. The NH₃-TPD peak area of the 1.0Pd-CeZrO_x catalyst decreased in the following order: 1.0Pd-CeZrO_x-CTAB > 1.0Pd-CeZrO_x-PM > 1.0Pd-CeZrO_x-CASG. Noteworthy, 1.0Pd-CeZrO_x-CTAB exhibited the largest desorption peak area, suggesting that the abundant weak acid sites were existent over the 1.0Pd-CeZrO_x-CTAB sample. The peak area ratio was used to determine the quantity of various acid sites (Table 3). The weak acid sites proportion over 1.0Pd-CeZrO_x-CTAB (88.33%) was higher than that of other samples. The 1.0Pd-CeZrO_x-CTAB sample had higher low-temperature catalytic activity in benzene and toluene catalytic oxidation, which might be assigned to the abundance of weak acid sites existent over 1.0Pd-CeZrO_x-CTAB.

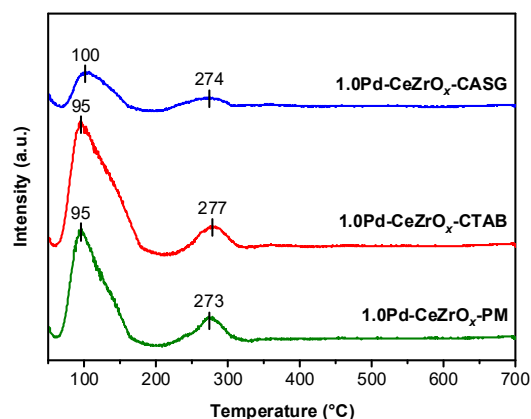


Figure 5. NH_3 -TPD results of 1.0Pd-CeZrO_x samples.

Table 3. The proportions of acid sites of 1.0Pd-CeZrO_x samples.

Sample	NH_3 Desorption Temperature ($^\circ\text{C}$)		Proportion of Acid Sites (%)	
	Weak	Moderate	Weak	Moderate
$1.0\text{Pd-CeZrO}_x\text{-CASG}$	95	277	88%	12%
$1.0\text{Pd-CeZrO}_x\text{-CTAB}$	100	274	80%	20%
$1.0\text{Pd-CeZrO}_x\text{-PM}$	95	273	82%	18%

3.4. Characterization of Oxygen Vacancies

Figure 6 shows the results of Raman, EPR, and XPS of 1.0Pd-CeZrO_x samples, which were further evaluated for the presence of oxygen vacancies. Figure 6a depicts the Raman spectra of 1.0Pd-CeZrO_x catalysts; the peak at 600 cm^{-1} is attributed to oxygen vacancies, whereas the peak at 460 cm^{-1} corresponds to the first-order F_{2g} peak in CeZrO_x samples, which indicates the integration of Zr^{4+} into the CeO_2 lattice [25,26]. And the characteristic peaks of tetragonal ZrO_2 occurred at 308 cm^{-1} [25,27]. The peak situated at around 638 cm^{-1} related to the B1 mode of PdO , which indicated the existence of Pd^{2+} species [28]. Subsequently, the oxygen vacancy concentration was then determined using the ratio of I_{600}/I_{455} . A higher I_{600}/I_{455} ratio indicates an increase in the concentration of oxygen defect sites [29]. The I_{600}/I_{455} ratio decreased in the order of $1.0\text{Pd-CeZrO}_x\text{-CTAB} > 1.0\text{Pd-CeZrO}_x\text{-PM} > 1.0\text{Pd-CeZrO}_x\text{-CASG}$, suggesting the higher oxygen vacancies concentration of the $1.0\text{Pd-CeZrO}_x\text{-CTAB}$ catalyst (Figure 6b). The existence of oxygen vacancies in the oxidation–reduction process improves the fluidity of O_2 and promotes materials' redox ability. The result is consistent with H_2 -TPR results; the $1.0\text{Pd-CeZrO}_x\text{-CTAB}$ sample exhibited the largest H_2 consumption and better redox performance.

EPR experiments could be additionally employed for identifying oxygen vacancies in 1.0Pd-CeZrO_x samples since the existence of oxygen vacancies induces the generation of paramagnetic species with unpaired electrons, which are especially highly responsive to EPR. For 1.0Pd-CeZrO_x samples (see Figure 6c), an obvious paramagnetic response signal at $g = 2.003$ was observed, corresponding to the oxygen vacancies species [30]. The three samples' EPR signal intensities varied from one to another; $1.0\text{Pd-CeZrO}_x\text{-CTAB}$ samples showed a strong signal of $g = 2.003$, demonstrating the highest amount of oxygen vacancies in this sample.

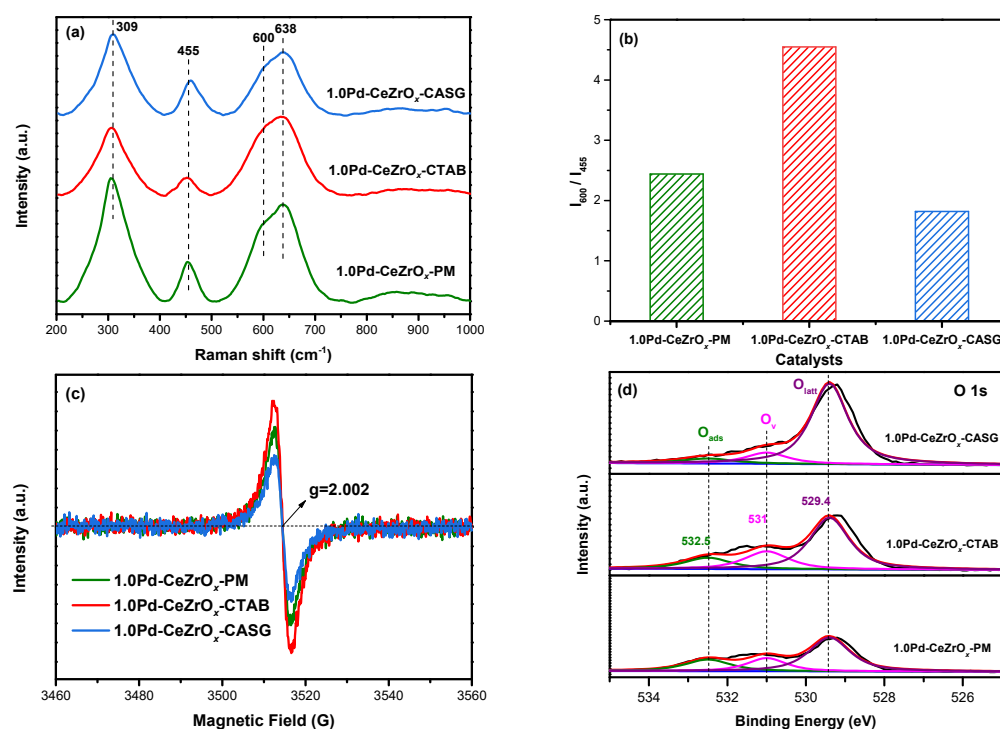


Figure 6. (a) Raman spectra; (b) the concentration of surface oxygen vacancies (I_{600}/I_{455}); (c) EPR spectra; and (d) XPS for O 1s of 1.0Pd-CeZrO_x catalysts.

O 1s spectra are frequently utilized for identifying the oxygen species. Figure 6d depicts the XPS spectrum of O 1s, and the proportion of different oxygen species could be estimated using the peak area ratio [31], as given in Table 4. Three distinct peaks that correspond to different kinds of oxygen species are apparent in the XPS O 1s spectra of 1.0Pd-CeZrO_x samples; lattice oxygen (O_{latt}) is represented by the peak at 529.4 eV, the band at 531 eV is assigned to the existence of oxygen vacancies (O_v), and chemisorbed oxygen species (O_{ads}) are denoted by the distinctive peak at higher binding energies (532.5 eV) [32,33]. Based on the peak area, the proportion of O_v of oxygen species ($O_v + O_{latt} + O_{ads}$) was calculated, and it was discovered that the sequence of oxygen vacancies proportion from high to low is 1.0Pd-CeZrO_x-CTAB > 1.0Pd-CeZrO_x-PM > 1.0Pd-CeZrO_x-CASG, suggesting that the 1.0Pd-CeZrO_x-CTAB sample had higher oxygen vacancies. The Raman, XPS, and O-XPS results show consistency. The maximum oxygen vacancy concentration is found in the 1.0Pd-CeZrO_x-CTAB sample, indicating that the catalytic activity of this material in catalytic degradation is higher than other samples [21].

Table 4. Surface atom concentrations of 1.0Pd-CeZrO_x catalysts.

Sample	Pd (at.%)	Ce (at.%)	Zr (at.%)	O (at.%)	Pd ²⁺ /Pd _{total}	Ce ³⁺ /Ce _{total}	$O_v/(O_v + O_{ads} + O_{latt})$
1.0Pd-CeZrO _x -CTAB	5.56	5.98	13.38	75.07	69.04%	30.15%	23.61%
1.0Pd-CeZrO _x -CASG	5.51	5.93	12.64	75.92	58.45%	22.37%	14.52%
1.0Pd-CeZrO _x -PM	6.61	6.45	14.51	72.43	70.00%	25.64%	21.24%

3.5. Analysis of Valence States

In order to better explore the redox ability of these samples, Figure 7a shows the H₂-TPR profiles of the 1.0Pd-CeZrO_x catalysts. The 1.0Pd-CeZrO_x-PM, 1.0Pd-CeZrO_x-CTAB, and 1.0Pd-CeZrO_x-CASG show reduction peaks at 97–100 °C, and the peaks are attributed to the stable PdO species, which has strong interaction between and support, as well as the reduction in Ce⁴⁺ species [28]. As for the 1.0Pd-CeZrO_x-PM sample, the reduction in PdO species to Pd⁰ is shown at 85 °C, but the 1.0Pd-CeZrO_x-CTAB catalyst shows a lower

reduction temperature (80 °C) than the 1.0Pd-CeZrO_x-PM catalyst, indicating that the 1.0Pd-CeZrO_x-CTAB sample is easily reduced [34]. In addition, the reduction temperatures of PdO on 1.0Pd-CeZrO_x-CTAB and 1.0Pd-CeZrO_x-CASG have a lower reduction temperature (49–50 °C), indicating that partial Pd species supported on 1.0Pd-CeZrO_x-CTAB and 1.0Pd-CeZrO_x-CASG are reduced more easily [21]. The H₂-TPR peak area of the 1.0Pd-CeZrO_x samples decreases in the following order: 1.0Pd-CeZrO_x-CTAB > 1.0Pd-CeZrO_x-PM > 1.0Pd-CeZrO_x-CASG. The 1.0Pd-CeZrO_x-CTAB catalyst has the best reducibility, and the higher redox properties imply the higher mobility of the oxygen species, which may result in the high catalytic oxidation activity in the benzene and toluene simultaneous oxidation. Furthermore, the H₂-TPR characterization results correspond with the activity results of the benzene and toluene conversion.

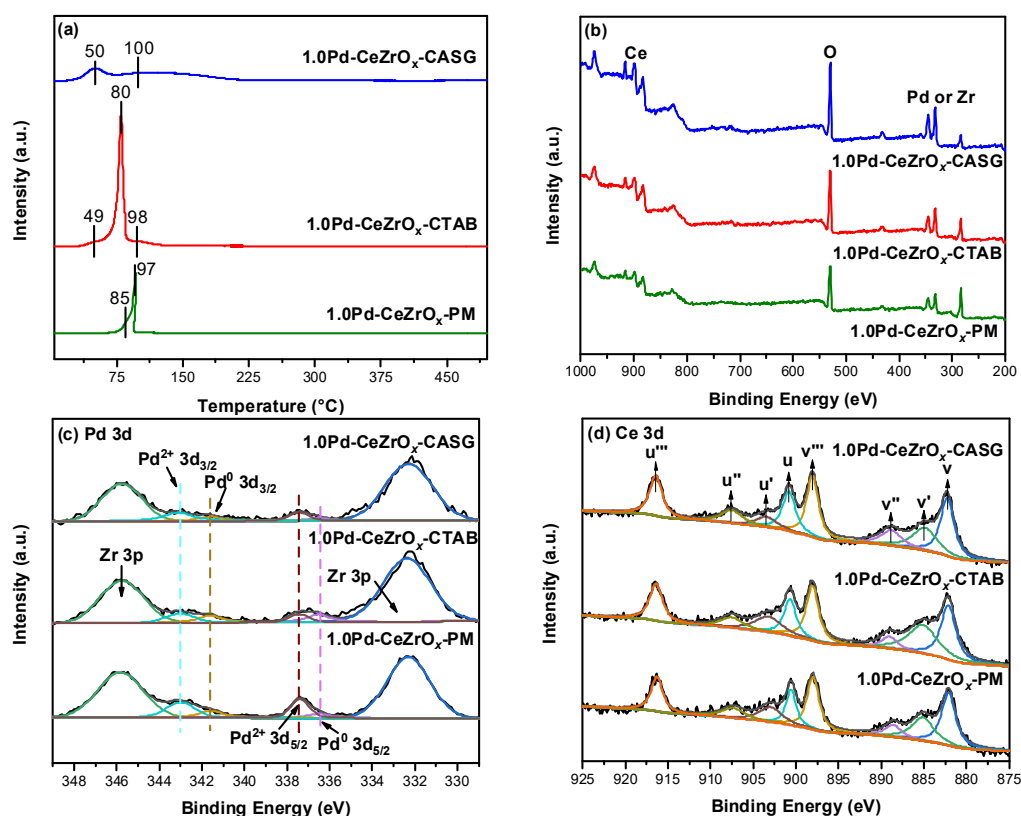


Figure 7. (a) H₂-TPR results; (b) XPS of survey spectrum; (c) Pd 3d; and (d) Ce 3d of 1.0Pd-CeZrO_x catalysts.

Figure 7c depicts the Pd 3d spectra of 1.0Pd-CeZrO_x catalysts; due to the overlap between the peaks of Zr 3p and Pd 3d, the separation of Pd 3d spectra were carried out, and it could be divided into four peaks [35,36]. The peaks situated at 343.1 and 337.4 eV, corresponding to 3d_{3/2} and 3d_{5/2} orbitals of Pd²⁺ species, and the peaks at 336.5 and 341.6 eV are ascribed to 3d_{5/2} and 3d_{3/2} orbitals of Pd⁰ species [37]. The proportions of Pd²⁺ and Pd^{total} were calculated corresponding to the peak area (see Table 4). The proportion of Pd²⁺ over 1.0Pd-CeZrO_x catalysts was ranked as 1.0Pd-CeZrO_x-PM (70.00%) > 1.0Pd-CeZrO_x-CTAB (69.04%) > 1.0Pd-CeZrO_x-CASG (58.45%). The activity assessment findings of the catalysts show that the synergistic catalytic oxidation performance of the 1.0Pd-CeZrO_x-PM and 1.0Pd-CeZrO_x-CTAB samples were better than that of 1.0Pd-CeZrO_x-CASG. As a result, it is hypothesized that the high valence Pd²⁺ species is the active center influencing the simultaneous catalytic elimination of benzene and toluene [38].

The Ce 3d spectra is shown in Figure 7d, which could be deconvoluted into eight peaks, corresponding to Ce³⁺ and Ce⁴⁺ species, respectively. The peaks at 884.2 eV and 904.3 eV are denoted as v' and u', which are ascribed to Ce³⁺ species. Other bands represented by v

(882.1 eV), v'' (888.1 eV), v''' (898.0 eV), u (900.3 eV), u'' (907.1 eV), and u''' (916.4 eV) are related to Ce^{4+} species [27,28]. The ratio of Ce^{3+}/Ce_{total} was calculated and is displayed in Table 4. The 1.0Pd-CeZrO_x-CTAB sample had the highest Ce^{3+}/Ce_{total} ratio (30.15%), which indicated more generation of oxygen vacancies in this sample. The results obtained from Ce 3d XPS are consistent with those obtained from Raman and EPR results. The development of each oxygen vacancy signifies the conversion of two Ce^{4+} to Ce^{3+} , and the free electrons created may increase the adsorption and activation of molecular oxygen, eventually increasing the catalyst's oxidation activity [39].

Based on the activity data, the performance of the 1.0Pd-CeZrO_x materials in the simultaneous oxidation of benzene and toluene is ranked from high to low as 1.0Pd-CeZrO_x-CTAB > 1.0Pd-CeZrO_x-PM > 1.0Pd-CeZrO_x-CASG, which corresponds to the proportion of oxygen vacancies. Therefore, it is speculated that oxygen vacancies influence the catalytic activity of the 1.0Pd-CeZrO_x samples. The oxygen vacancy concentration of 1.0Pd-CeZrO_x-CTAB materials is relatively high, and there are also highly active Pd²⁺ species that promote the adsorption activation and subsequent reaction of reactant molecules on the sample surface.

4. Conclusions

In conclusion, CeZrO_x samples were synthesized by different methods, with Pd as an active component loaded onto CeZrO_x by the impregnation method. The 1.0Pd-CeZrO_x samples were successfully produced and used to simultaneously eliminate benzene and toluene. It is demonstrated that the preparation procedure of CeZrO_x has a considerable impact on the catalytic activity. The benzene and toluene conversion of the 1.0Pd-CeZrO_x samples increase in the following order: 1.0Pd-CeZrO_x-CASG < 1.0Pd-CeZrO_x-PM < 1.0Pd-CeZrO_x-CTAB. The 1.0Pd-CeZrO_x-CTAB catalyst could achieve synergistic oxidation of benzene and toluene at 250 °C, while CO₂ selectivity reaches 100%. The superior catalytic activity of the 1.0Pd-CeZrO_x-CTAB sample related to the higher redox properties of this sample, as confirmed in H₂-TPR, O-XPS, Raman, and EPR results indicate that the high amount of oxygen vacancies in 1.0Pd-CeZrO_x-CTAB are responsible for catalytic activity. And the large amount of surface Pd²⁺ species may operate as active centers, impacting the simultaneous catalytic oxidation of benzene and toluene. Additionally, NH₃-TPD results reveal that the 1.0Pd-CeZrO_x-CTAB sample has weak acid sites existent, which might be beneficial for the adsorption and reaction of pollutants. This study provides high-performance materials for the simultaneous elimination of benzene and toluene, expanding catalyst preparation sights for the removal of benzene and toluene.

Author Contributions: Conceptualization, D.L.; Formal analysis, D.L.; Investigation, X.X., Y.W. and M.H.; Data curation, Y.W. and Z.L.; Writing—original draft, X.X.; Writing—review & editing, Z.L. and K.Y.; Supervision, D.L.; Funding acquisition, X.X. and K.Y. All authors have read and agreed to the published version of the manuscript.

Funding: This research was funded by National Natural Science Foundation of China grant numbers [22206146, 22006079].

Institutional Review Board Statement: Not applicable.

Informed Consent Statement: Not applicable.

Data Availability Statement: The datasets used in this study will be available from the corresponding author upon reasonable request.

Conflicts of Interest: The authors declare no conflict of interest.

References

1. Liu, W.; Zhang, Z.; Yuan, K.; Dang, D.; Jin, P.; Han, X.; Ge, Q. Catalytic Oxidation Degradation of Volatile Organic Compounds (VOCs)—A Review. *Rev. Inorg. Chem.* **2024**, *44*, 209–229. [[CrossRef](#)]
2. Ding, S.; Wu, S.; Fang, N.; Chu, Y.; Wang, P.; Ding, L. Design and Synthesis of Porous Nano-Confined Catalysts for VOCs Oxidation: A Critical Review Based on Pollutant Sorts. *Sep. Purif. Technol.* **2025**, *352*, 128158. [[CrossRef](#)]

3. Gao, W.; Tang, X.; Yi, H.; Jiang, S.; Yu, Q.; Xie, X.; Zhuang, R. Mesoporous Molecular Sieve-Based Materials for Catalytic Oxidation of VOC: A Review. *J. Environ. Sci.* **2023**, *125*, 112–134. [[CrossRef](#)] [[PubMed](#)]
4. Zhang, H.; Wang, Z.; Wei, L.; Liu, Y.; Dai, H.; Deng, J. Recent Progress on VOC Pollution Control via the Catalytic Method. *Chin. J. Catal.* **2024**, *61*, 71–96. [[CrossRef](#)]
5. Meng, F.; Tang, X.; Kadja, G.T.M.; Yi, H.; Zhao, S.; Wu, W.; Zhang, Y.; Gao, F.; Yu, Q. A Systematic Review with Improving Activity and Stability in VOCs Elimination by Oxidation of Noble Metals: Starting from Active Sites. *Sep. Purif. Technol.* **2025**, *354*, 129222. [[CrossRef](#)]
6. Guo, X.; Shi, Y.; Zhou, A.; Wang, Y.; Zhou, R. Challenging Design of Highly Active Pt/CeO₂-TiO₂/ZSM-5 Catalysts for VOCs Low-Temperature Removal. *Mater. Today Sustain.* **2024**, *27*, 100938. [[CrossRef](#)]
7. Zhou, B.; Ke, Q.; Wen, M.; Ying, T.; Cui, G.; Zhou, Y.; Gu, Z.; Lu, H. Catalytic Combustion of Toluene on Pt/Al₂O₃ and Pd/Al₂O₃ Catalysts with CeO₂, CeO₂-Y₂O₃ and La₂O₃ as Coatings. *J. Rare Earths* **2023**, *41*, 1171–1178. [[CrossRef](#)]
8. Cui, J.; Cui, Y.; Tan, J.; Zhang, H.; Gu, M.; Huang, L. Efficient Catalytic Oxidation of VOCs by a Pd-Pt/SiO₂ Catalyst: The Cooperative Catalysis of Dual Metal Sites. *J. Environ. Chem. Eng.* **2024**, *12*, 111930. [[CrossRef](#)]
9. Zhou, W.; Li, H.; Song, B.; Ma, W.; Liu, Z.; Wang, Z.; Xu, Z.; Meng, L.; Wang, Y.; Qin, X.; et al. Catalytic Oxidation Mechanism of Toluene over Ce_xMn_{1-x}O₂: The Role of Oxygen Vacancies in Adsorption and Activation of Toluene. *Langmuir* **2023**, *39*, 8503–8515. [[CrossRef](#)]
10. Zhang, Y.; Wu, C.; Wang, Z.; Ji, J.; Wan, H.; Zou, W.; Tong, Q.; Sun, J.; Dong, L.; Chen, Y.-W. Enhanced Low-Temperature Catalytic Performance for Toluene Combustion of CeO₂-Supported Pt-Ir Alloy Catalysts. *Appl. Surf. Sci.* **2022**, *580*, 152278. [[CrossRef](#)]
11. Wang, L.; Sun, Y.; Ma, Y.; Xu, M.; Zhang, J.; Zhu, Y.; Ding, J.; Zhu, L.; Ma, J.; Ji, W.; et al. Electron Donation Promotes the Dual Activation of Lattice Oxygen and Molecular Oxygen: The Pt-Pd/CeO₂ Catalyst Efficiently Catalyzes Toluene. *J. Catal.* **2023**, *428*, 115133. [[CrossRef](#)]
12. Yang, Z.; Hu, W.; Zhang, N.; Li, Y.; Liao, Y. Facile Synthesis of Ceria-Zirconia Solid Solutions with Cubic-Tetragonal Interfaces and Their Enhanced Catalytic Performance in Diesel Soot Oxidation. *J. Catal.* **2019**, *377*, 98–109. [[CrossRef](#)]
13. Ouyang, J.; Zhao, Z.; Yang, H.; He, J.; Suib, S.L. Surface Redox Characters and Synergetic Catalytic Properties of Macroporous Ceria-Zirconia Solid Solutions. *J. Hazard. Mater.* **2019**, *366*, 54–64. [[CrossRef](#)] [[PubMed](#)]
14. Deng, Q.-F.; Ren, T.-Z.; Agula, B.; Liu, Y.; Yuan, Z.-Y. Mesoporous Ce_xZr_{1-x}O₂ Solid Solutions Supported CuO Nanocatalysts for Toluene Total Oxidation. *J. Ind. Eng. Chem.* **2014**, *20*, 3303–3312. [[CrossRef](#)]
15. Wang, J.; Lai, X.; Zhang, H.; Zhou, X.; Lin, T.; Wang, J.; Chen, Y. Low-Temperature Toluene Oxidation on Ag/Ce_xZr_{1-x}O₂ Monolithic Catalysts: Synergistic Catalysis of Silver and Ceria-Zirconia. *Combust. Flame* **2023**, *248*, 112577. [[CrossRef](#)]
16. Zheng, Z.; Wu, S.; Huang, Z.; Xu, H.; Shen, W. Insights into Enhancing SO₂ Tolerance for Catalytic Combustion of Toluene over Sulfated CeZrO_x Supported Platinum Catalysts. *Colloids Surf. A Physicochem. Eng. Asp.* **2023**, *669*, 131539. [[CrossRef](#)]
17. Meng, F.; Li, X.; Zhang, P.; Yang, L.; Liu, S.; Li, Z. A Facile Approach for Fabricating Highly Active ZrCeZnO in Combination with SAPO-34 for the Conversion of Syngas into Light Olefins. *Applied Surface Science* **2021**, *542*, 148713. [[CrossRef](#)]
18. Mikhail, M.; Da Costa, P.; Amouroux, J.; Cavadias, S.; Tatoulian, M.; Ognier, S.; Gálvez, M.E. Electrocatalytic Behaviour of CeZrO_x-Supported Ni Catalysts in Plasma Assisted CO₂ Methanation. *Catal. Sci. Technol.* **2020**, *10*, 4532–4543. [[CrossRef](#)]
19. Kunkes, E.L.; Gürbüz, E.I.; Dumesic, J.A. Vapour-Phase C-C Coupling Reactions of Biomass-Derived Oxygenates over Pd/CeZrO_x Catalysts. *J. Catal.* **2009**, *266*, 236–249. [[CrossRef](#)]
20. Liu, J.; Zhao, M.; Xu, C.; Liu, S.; Zhang, X.; Chen, Y. Ultrasonic-Assisted Fabrication and Catalytic Activity of CeZrAl Oxide-Supported Pd for the Purification of Gasohol Exhaust. *Chin. J. Catal.* **2013**, *34*, 751–757. [[CrossRef](#)]
21. Wang, M.; Kim, S.Y.; Men, Y.; Shin, E.W. Influence of Metal-Support Interactions on Reaction Pathways over Ni/CeZrO_x-Al₂O₃ Catalysts for Ethanol Steam Reforming. *Int. J. Hydrogen Energy* **2022**, *47*, 33765–33780. [[CrossRef](#)]
22. Xu, H.; Feng, X.; Liu, S.; Wang, Y.; Sun, M.; Wang, J.; Chen, Y. Promotional Effects of Titanium Additive on the Surface Properties, Active Sites and Catalytic Activity of W/CeZrO_x Monolithic Catalyst for the Selective Catalytic Reduction of NO_x with NH₃. *Appl. Surf. Sci.* **2017**, *419*, 697–707. [[CrossRef](#)]
23. Li, M.; Zhang, X.; Liu, X.; Lian, Y.; Niu, X.; Zhu, Y. Excellent Low-Temperature Activity for Oxidation of Benzene Series VOCs over Hollow Pt/CoMn₂O₄ Sub-Nanosphere: Synergistic Effect between Pt and CoMn₂O₄ on Improving Oxygen Activation. *Chem. Eng. J.* **2023**, *473*, 145478. [[CrossRef](#)]
24. Ma, S.; Hou, Y.; Li, Y.; Ding, X.; Yang, Y.; Tian, J.; Cui, Y.; Huang, Z. Regulation of A-Site Cations in AMn₂O_x Spinel Catalysts on the Deep Oxidation of Light Alkanes VOCs. *Fuel* **2023**, *334*, 126785. [[CrossRef](#)]
25. Sellick, D.R.; Aranda, A.; García, T.; López, J.M.; Solsona, B.; Mastral, A.M.; Morgan, D.J.; Carley, A.F.; Taylor, S.H. Influence of the Preparation Method on the Activity of Ceria Zirconia Mixed Oxides for Naphthalene Total Oxidation. *Appl. Catal. B Environ.* **2013**, *132–133*, 98–106. [[CrossRef](#)]
26. Wang, Y.; Yu, H.; Hu, Q.; Huang, Y.; Wang, X.; Wang, Y.; Wang, F. Application of Microimpinging Stream Reactor Coupled with Ultrasound in Cu/CeZrO_x Solid Solution Catalyst Preparation for CO₂ Hydrogenation to Methanol. *Renew. Energy* **2023**, *202*, 834–843. [[CrossRef](#)]
27. Zhao, Y.; Wang, W.; Yin, X.; Wang, L.; Li, S.; Wang, J.; Chen, Y. Engineering Excellent Pd/CeO₂-ZrO₂-Al₂O₃ Catalyst with Abundant Oxygen Vacancies by Pr Surface Modification for Eliminating NO and C₃H₈. *J. Alloys Compd.* **2023**, *938*, 168585. [[CrossRef](#)]

28. Li, S.; Zhang, H.; Dan, Y.; Deng, J.; Wang, J.; Xiong, L.; Chen, Y. Design and Synthesize Highly Active Pd-Only Three-Way Catalyst by Optimizing the Reducibility of CeO₂-ZrO₂-Al₂O₃ Support. *Mol. Catal.* **2020**, *482*, 110696. [[CrossRef](#)]
29. Wang, Z.; Sun, X.; Liu, J.; Li, X. The NO Oxidation Performance over Cu/Ce_{0.8}Zr_{0.2}O₂ Catalyst. *Surf. Interfaces* **2017**, *6*, 103–109. [[CrossRef](#)]
30. Kang, X.; Dong, G.; Dong, T. Oxygen Vacancy Defect Engineering of Heterophase Junction TiO₂: Interfacial/Surface Oxygen Vacancies Coadjust the Photocatalytic ROS Production. *ACS Appl. Energy Mater.* **2023**, *6*, 1025–1036. [[CrossRef](#)]
31. Sun, W.; Li, X.; Mu, J.; Fan, S.; Yin, Z.; Wang, X.; Qin, M.; Tadé, M.; Liu, S. Improvement of Catalytic Activity over Mn-Modified CeZrO Catalysts for the Selective Catalytic Reduction of NO with NH₃. *J. Colloid Interface Sci.* **2018**, *531*, 91–97. [[CrossRef](#)] [[PubMed](#)]
32. Wu, Y.; Lu, Y.; Song, C.; Ma, Z.; Xing, S.; Gao, Y. A Novel Redox-Precipitation Method for the Preparation of α-MnO₂ with a High Surface Mn⁴⁺ Concentration and Its Activity toward Complete Catalytic Oxidation of o-Xylene. *Catal. Today* **2013**, *201*, 32–39. [[CrossRef](#)]
33. Wu, Y.; Zhang, Y.; Liu, M.; Ma, Z. Complete Catalytic Oxidation of O-Xylene over Mn–Ce Oxides Prepared Using a Redox-Precipitation Method. *Catal. Today* **2010**, *153*, 170–175. [[CrossRef](#)]
34. Li, L.; Zhang, N.; He, H.; Zhang, G.; Song, L.; Qiu, W. Shape-Controlled Synthesis of Pd Nanocrystals with Exposed {110} Facets and Their Catalytic Applications. *Catal. Today* **2019**, *327*, 28–36. [[CrossRef](#)]
35. Wang, G.; You, R.; Meng, M. An Optimized Highly Active and Thermo-Stable Oxidation Catalyst Pd/Ce–Zr–Y/Al₂O₃ Calcined at Superhigh Temperature and Used for C₃H₈ Total Oxidation. *Fuel* **2013**, *103*, 799–804. [[CrossRef](#)]
36. Zhao, X.; Wang, Y.; Zheng, Z.; Zhang, Y.; Li, K.; Chen, T.; Guo, D.; Cao, H.; Zhan, R.; Lin, H. Comparative Study on Properties of Pd-Ce-Zr Catalysts Synthesized by Flame Spray Pyrolysis and Solution Combustion: Application for Methane Catalytic Oxidation in Electric Field. *Appl. Surf. Sci.* **2021**, *566*, 150536. [[CrossRef](#)]
37. Zhang, Y.; Zhang, C.; Liu, G.; Wang, L.; Pan, Z. Ce-Doped SBA-15 Supported Pd Catalyst for Efficient Hydrogenation of 2-Ethyl-Anthraquinone. *Appl. Surf. Sci.* **2023**, *616*, 156515. [[CrossRef](#)]
38. Ruzzi, P.; Salusso, D.; Baravaglio, M.; Szeto, K.C.; De Mallmann, A.; Jiménez, L.G.; Godard, C.; Benayad, A.; Morandi, S.; Bordiga, S.; et al. Supported PdZn Nanoparticles for Selective CO₂ Conversion, through the Grafting of a Heterobimetallic Complex on CeZrO_x. *Appl. Catal. A Gen.* **2022**, *635*, 118568. [[CrossRef](#)]
39. Deka, D.J.; Pihl, J.A.; Thomas, C.R.; Partridge, W.P. Intra-Catalyst CH₄ Oxidation Pathways on a Pd/Al₂O₃/CeZrO_x-Based Commercial Catalyst and Implications on NO_x Conversion Profiles for a Natural Gas Vehicle Exhaust under Lambda Modulation. *Chem. Eng. J.* **2023**, *472*, 144803. [[CrossRef](#)]

Disclaimer/Publisher’s Note: The statements, opinions and data contained in all publications are solely those of the individual author(s) and contributor(s) and not of MDPI and/or the editor(s). MDPI and/or the editor(s) disclaim responsibility for any injury to people or property resulting from any ideas, methods, instructions or products referred to in the content.